

The Origin of Spin-Alignment of Dark Matter Subhalos

DAIKI OSAFUNE ,¹ KEIICHI WADA ,^{2,3,4} TOMOAKI ISHIYAMA ,⁵ AND TAKASHI OKAMOTO ,⁴

¹Department of Cosmosciences, Graduates School of Science, Hokkaido University, N10 W8, Kitaku, Sapporo, 060-0810, Japan

²Graduate School of Science and Engineering, Kagoshima University, Kagoshima 890-0065, Japan

³Research Center for Space and Cosmic Evolution, Ehime University, Matsuyama 790-8577, Japan

⁴Department of Physics, Faculty of Science, Hokkaido University, N10 W8, Kitaku, Sapporo 060-0810, Japan

⁵Digital transformation enhancement council, Chiba University, 1-33, Yayoi-cho, Inage-ku, Chiba, 263-8522, Japan

ABSTRACT

Subhalo spin is essential for modeling galaxy formation and controlling systematic uncertainties in intrinsic alignment (IA) studies. However, the physical mechanisms governing subhalo spin acquisition within the tidal environments of host halos remain poorly understood. In this work, we investigate the alignment between subhalo and host halo spins using the high-resolution cosmological *N*-body simulation, Shin-Uchuu. We find that the spin alignment between subhalos and host halos becomes increasingly pronounced toward the central regions. Our analysis reveals that subhalos typically acquire spin in the same direction as their orbital angular momentum. Since the orbital angular momentum of most subhalos is aligned with the host halo spin, an overall alignment between subhalo and host spins emerges. When classified by orbital orientation, however, subhalo spins in the inner regions are found to be oriented perpendicularly or anti-parallel to the host spin for polar and retrograde orbits, respectively. These results provide strong evidence that subhalo spins are acquired through torques exerted by the tidal field of the host halo. Furthermore, we demonstrate that the mass ratio and the radial distance from the host center are the primary parameters governing subhalo spin alignment, while the dependence on the accretion redshift is found to be negligible.

Keywords: N-body simulations (1083) — Galaxy dark matter halos (1880) — Galaxy kinematics (602) — Galaxy interactions (600)

1. INTRODUCTION

In the standard cosmological model, halos form via gravitational instability of initial dark matter density fluctuations and grow through the merger and accretion of other halos. When a smaller halo accretes onto a more massive halo, it is referred to as a subhalo, while the larger system is termed its host halo. Subhalos are subsequently tidally stripped and disrupted by the tidal field of the host halo (F. C. van den Bosch et al. 2005; M. Boylan-Kolchin et al. 2008). The presence of subhalos is observable through gravitational lensing (P. Natarajan et al. 2009) and the kinematics of satellite galaxies (R. G. Carlberg 2012).

Weak gravitational lensing serves as a powerful tool for probing the mass distribution and internal structures of galaxies (N. Okabe et al. 2014; K. T. Inoue et al. 2015; C. Sifón et al. 2018; W. Luo et al. 2018; C. Hikage et al.

2019; V. Ghirardini et al. 2024; M. Fujikawa & M. Oguri 2025).

The intrinsic correlation of galaxy shapes and orientations with the surrounding gravitational field is known as intrinsic alignments (IA). Understanding IA is crucial for ensuring the precision and reliability of weak lensing surveys (e.g., B. Joachimi et al. 2015, for a review). Especially on small scales ($\lesssim 1\text{Mpc}$), accounting for the IA of subhalos and satellite galaxies within central galaxy halos improves the precision of the analysis (N. Van Alfen et al. 2024). In early type galaxies, the intrinsic alignment of galaxy is often described by models based on the linear alignment framework which considers the shapes and ellipticities of galaxies (C. M. Hirata & U. Seljak 2004). In contrast, for late type galaxies and subhalos, analyses that account for the influence of tidal torques induced by the surrounding tidal field have been proposed (J. Lee & U.-L. Pen 2008; S. Codis et al. 2015). It is thought that tidal forces influence the orientation of the major axis, and observational and

theoretical studies discovered a tendency for the major axis of subhalos to point towards the centre of the host halo (M. J. Pereira et al. 2008; A. Knebe et al. 2008, 2020; P. Wang et al. 2019). Although this trend is generally attributed to tidal torques, its detailed physical mechanism is not clear.

Previous research suggests that the effect of tidal torques from the host halo extends not only to the shape of subhalos but also to their spin. Theoretical and observational studies have shown a tendency for the spin vectors of subhalos to align with those of their host halos (D. Aubert et al. 2004; C. Welker et al. 2018; P. Wang 2025) and these results further suggest that this spin alignment is related to the properties of satellite galaxies, such as their color, morphology, and stellar mass, implying a connection with their formation histories. Despite these findings, the specific physical origin of subhalo spin alignment remains elusive, largely due to the insufficient mass resolution and limited sample sizes of existing studies. For example, C. Welker et al. (2018) analyzed a stacked sample within $0.3 < z < 0.8$ with a box size of $L = 100 h^{-1} \text{cMpc}$, which may not provide the detailed small-scale dynamics or statistical robustness required for a comprehensive investigation.

In this study, we investigate the statistical properties induced by tidal torques from host halos using snapshots of the high-resolution cosmological N -body simulation, Shin-Uchuu which features a box size of $L = 140 h^{-1} \text{cMpc}$ and 100 times higher dark matter mass resolution than the simulation used in C. Welker et al. (2018). The improvements in both resolution and sample size now allow for robust statistical investigations of subhalos, even after imposing multiple parameter constraints. By analyzing the relationship between subhalo spin and the distance from the host halo center under constraints of some parameter, this study aims to elucidate how the tidal field of the host halo influences subhalo properties.

This paper is organised as follows. Details of our simulations, sample selection, and analysis method are described in Section 2. In Section 3, we present the statistical results on the alignment of subhalo spins and orbital angular momenta. Finally, we provide a discussion and conclusions in Section 4.

2. DATA AND ANALYSIS

2.1. Cosmological N -body simulation data

We use a cosmological N -body simulation, Shin-Uchuu (T. Ishiyama et al. 2021). The cosmological simulation consists of $N = 6400^3$ dark matter particles in a comoving cubic box of size $L = 140.0 h^{-1} \text{cMpc}$. The particle mass is $m_p = 8.97 \times 10^5 h^{-1} M_\odot$ and the softening length is $\epsilon = 0.4 h^{-1} h^{-1} \text{ckpc}$. The cosmo-

logical parameters are $\Omega_0 = 0.3089$, $\Omega_b = 0.0486$, $\lambda_0 = 0.6911$, $h = 0.6774$, $n_s = 0.9667$, and $\sigma_8 = 0.8159$ (Planck Collaboration et al. 2020).

Halos/subhalos are identified by ROCKSTAR⁶ halo finder (P. S. Behroozi et al. 2013a), which outputs physical properties such as position, velocity and angular momentum of halos. The angular momentum of subhalo (host halo) $\vec{J}_{\text{sub(host)}}$ is calculated from the positions, r_i of halo and masses, m_i , and velocities, \vec{v}_i of its constituent particles as follows:

$$\vec{J}_{\text{sub(host)}} = \sum_{i=1}^N m_i (\vec{r}_i \times \vec{v}_i) \quad (1)$$

The merger trees are constructed by CONSISTENT TREES⁷ (P. S. Behroozi et al. 2013b) based on the data that output from ROCKSTAR at each redshift. The halo and subhalo catalogues are available on the Skies & Universes site.⁸ We analyze subhalos at $z = 0$ that consist of at least 1,000 dark matter particles and reside in distinct host halos. This selection ensures the numerical robustness of measured physical properties and mitigates the influence of complex dynamics within nested hierarchical structures. The sample of subhalos at $z = 0$ used in this study consists of $N_{\text{sub}} = 1.13 \times 10^6$, with the minimum and maximum mass are $M_{\text{min}} = 8.97 \times 10^8 h^{-1} M_\odot$ and $M_{\text{max}} = 1.69 \times 10^{14} h^{-1} M_\odot$, respectively. Similarly, the host halo sample includes $N_{\text{host}} = 3.07 \times 10^5$, with masses ranging from $M_{\text{min}} = 9.26 \times 10^8 h^{-1} M_\odot$ to $M_{\text{max}} = 1.23 \times 10^{15} h^{-1} M_\odot$. To examine the evolution of subhalos, we used merger trees to analyze subhalos that survive at $z = 0$, tracing their history from the redshift of accretion to $z = 0$. Since only a small number of subhalos accreted at $z > 2$ survive until $z = 0$, we focused exclusively on the sample accreted at $z < 2$.

To investigate the various alignments, we will analyze the cosine values of the angles defined by the following quantities:

- The alignment between the spin of subhalos and their host halos ($\cos \theta$).
- The alignments between the orbital angular momentum of the subhalos, \vec{J}_{orb} and the spin of both the subhalos ($\cos \phi$) and the host halos ($\cos \eta$).
- The positional alignment of subhalos relative to the spin direction of host halo ($\cos \chi$).

⁶ <https://bitbucket.org/gfcstanford/rockstar/>

⁷ <https://bitbucket.org/pbehroozi/consistent-trees/>

⁸ <https://www.skiesanduniverses.org/Simulations/Uchuu/>

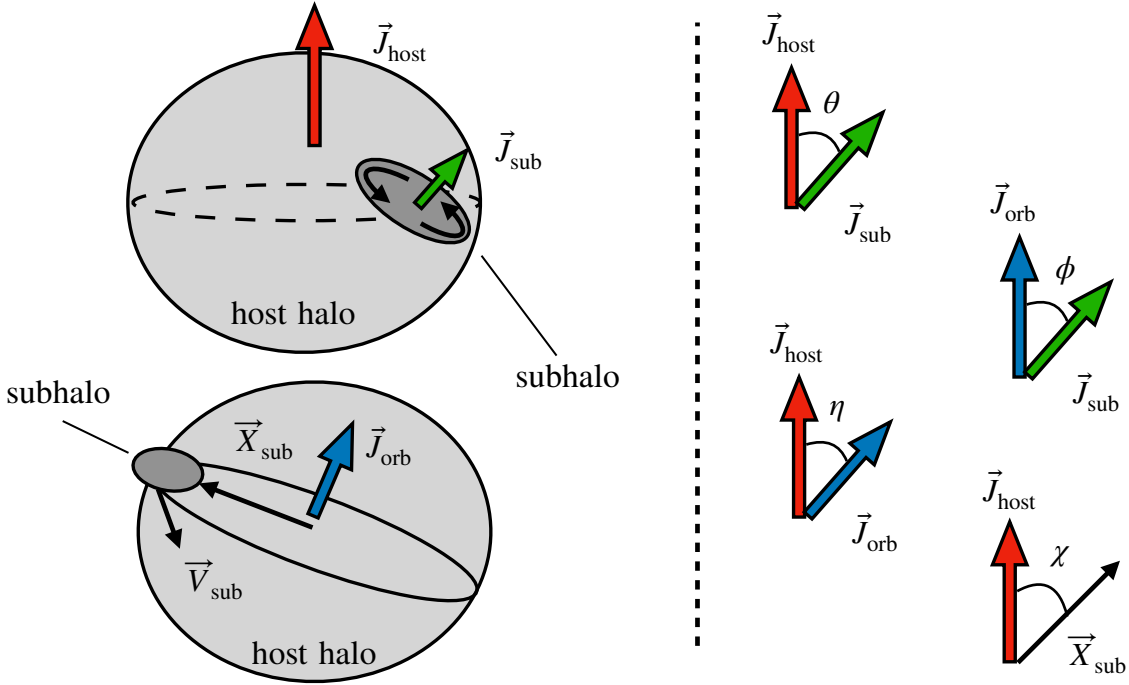


Figure 1. Schematic illustration of the vectors and the alignments of subhalo and host halo used for this study.

These alignments are illustrated in Figure 1 and defined by the following equations:

$$\cos \theta \equiv \frac{\vec{J}_{\text{sub}} \cdot \vec{J}_{\text{host}}}{|\vec{J}_{\text{sub}}| |\vec{J}_{\text{host}}|} \quad (2)$$

$$\cos \phi \equiv \frac{\vec{J}_{\text{sub}} \cdot \vec{J}_{\text{orb}}}{|\vec{J}_{\text{sub}}| |\vec{J}_{\text{orb}}|} \quad (3)$$

$$\cos \eta \equiv \frac{\vec{J}_{\text{orb}} \cdot \vec{J}_{\text{host}}}{|\vec{J}_{\text{orb}}| |\vec{J}_{\text{host}}|} \quad (4)$$

$$\cos \chi \equiv \frac{\vec{X}_{\text{sub}} \cdot \vec{J}_{\text{host}}}{|\vec{X}_{\text{sub}}| |\vec{J}_{\text{host}}|} \quad (5)$$

where (\cdot) denotes the inner product operation. The orbital angular momentum of subhalos, \vec{J}_{orb} is calculated from the subhalo's position (\vec{X}_{sub}), mass (M_{sub}), and velocity (\vec{V}_{sub}) relative to the host halo, which are output by ROCKSTAR:

$$\vec{J}_{\text{orb}} = M_{\text{sub}} (\vec{X}_{\text{sub}} \times \vec{V}_{\text{sub}}) \quad (6)$$

Focusing on these quantities, and the distance from the center of the host halo normalised by its virial radius (R_{vir}), we investigate the influence of the host halo on the alignment of the subhalos.

3. RESULTS

3.1. Angle between angular momentum of subhalo and host halo

Figure 2 shows the distribution of the distance from the center of the host halos, r/R_{vir} , and the spin alignment between subhalo and host halo, $\cos \theta$. The left panel presents a two-dimensional (2D) histogram of these quantities, with the median and the interquartile range (25th to 75th percentiles) of $\cos \theta$ overlaid for each radial bin to highlight the average trend. At the outskirts of the host halo, the median value of $\cos \theta$ is close to zero, and interquartile range (25th to 75th percentiles) is approximately ± 0.5 , indicating little to no preferred alignment. However, both the median and the overall distribution of $\cos \theta$ increase toward the center, demonstrating a clear tendency for subhalo spin directions to become more aligned with that of the host halo in the inner regions.

The right panel of Figure 2 shows the probability distribution function (PDF) of $\cos \theta$, where the values on the vertical axis represent the excess probability relative to a uniform distribution. We present results for the full sample and three subsamples binned by their distance from the host halo center r/R_{vir} . The full sample reveals a statistical tendency for subhalo and host halo spins to align. Furthermore, the alignment is close to a uniform distribution at the outskirts of host halos, whereas it becomes progressively stronger toward the central regions.

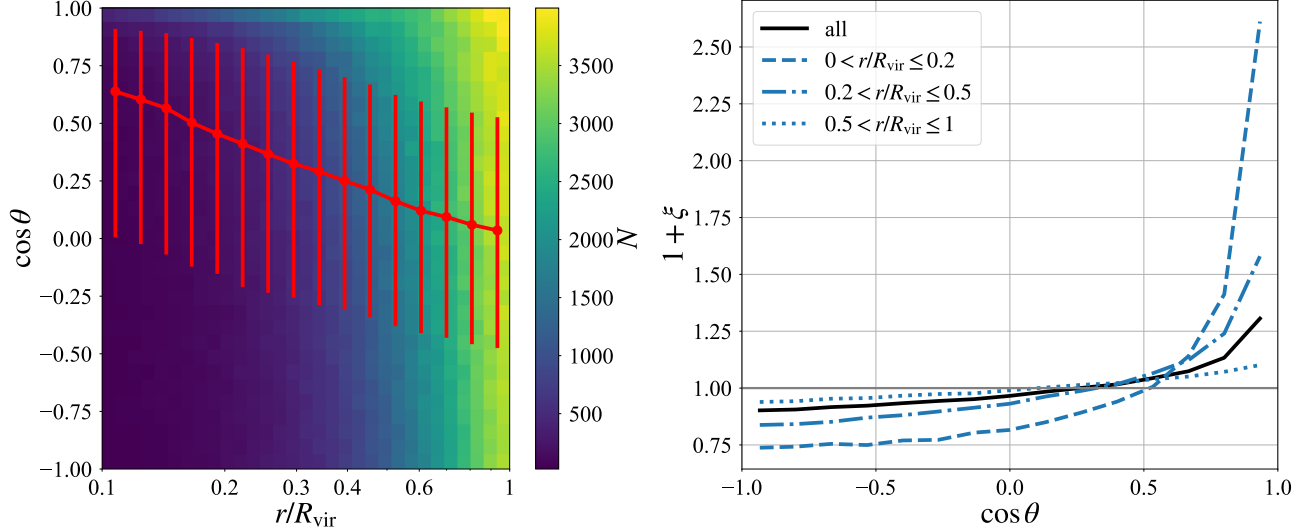


Figure 2. Left : A 2D histogram of the angle between the spin of the subhalos and the host halos, $\cos \theta$, and the distance from the center of the host halos, r/R_{vir} . The red lines indicate the median, and the 25th and 75th percentiles. Right : PDF of $\cos \theta$, y-axis shows the deviation from a uniform probability distribution. Data are the full sample (black line) and subsample by r/R_{vir} (blue lines).

This is consistent with the results of previous studies (D. Aubert et al. 2004; C. Welker et al. 2018), which focus on the spin alignment between the satellite and host galaxies.

Figure 3 shows the relationship between r/R_{vir} and $\cos \theta$, subsampled by subhalo to host halo mass ratio, $M_{\text{sub}}/M_{\text{host}}$. The upper panels show the 2D histograms and the lower panels show the PDFs of the subsample. As indicated by the median values of $\cos \theta$ at each r/R_{vir} and the PDFs, the spin alignment between subhalos and host halos becomes more pronounced as the mass ratio increases.

The radial distribution of subhalos depends strongly on the mass ratio. As indicated by the color scale in the 2D histogram, subhalos with small mass ratios $10^{-3} \leq M_{\text{sub}}/M_{\text{host}} < 10^{-2}$ are primarily located in the outskirts of the host halo. In contrast, those with large mass ratios $10^{-1} \leq M_{\text{sub}}/M_{\text{host}} < 1$ are concentrated around $r/R_{\text{vir}} \sim 0.4$ and $\cos \theta \sim 1$. This is because subhalos with higher mass ratios relative to their host halos experience stronger dynamical friction, causing them to sink toward the center on shorter timescales. Consequently, the alignment observed in the central regions in Figure 2 (without mass-ratio binning) is dominated by the contribution of high-mass-ratio subhalos.

3.2. Subhalo Spin Alignment and Orbital Motion

In the previous section, a tendency for the spin of subhalos and host halos to align was observed. If this alignment originates from tidal torques exerted by the host halo (D. Aubert et al. 2004; O. Hahn et al. 2007; M. R. Lovell et al. 2011), the spin of the subhalos is ex-

pected to align with the direction of their orbital angular momentum. We thus investigate the alignment between the spin and orbital angular momentum of the subhalo, $\cos \phi$. Figure 4 is formatted similarly to Figure 2, but the vertical axis of the 2D histogram and the horizontal axis of the PDF represent the angle between spin and orbital angular momentum of subhalo, $\cos \phi$. Figure 4 shows that, similarly to Figure 2, the tendency toward alignment is stronger toward the center of the host halo. Furthermore, the PDF values for $\cos \phi > 0.5$ exceed those for $\cos \phi > 0.5$, indicating that the alignment between subhalo orbital angular momentum and spin is stronger than the alignment between subhalo and host halo spins. The alignment between subhalo spin and orbital angular momentum is physically consistent with a scenario where subhalos acquire their spin via tidal torquing within the host halo environment.

If this scenario is correct, the trend of spin alignment is expected to vary depending on the orbital orientation of the subhalos. We therefore investigate the relationship between $\cos \theta$ and r/R_{vir} by categorizing subhalos into different orbital types. We classify subhalos located near the equatorial plane of the host halo ($|\cos \chi| < 0.5$) into three orbital categories, based on the alignment between their orbital angular momentum and that of the host halo’s spin ($\cos \eta$). These categories are defined as retrograde ($-1 \leq \cos \eta < -1/3$), polar ($-1/3 \leq \cos \eta \leq 1/3$), and prograde ($1/3 < \cos \eta \leq 1$). A classification based solely on $\cos \eta$ cannot distinguish whether a subhalo at $\cos \chi \approx 1$ is in a genuine polar orbit or is a subhalo from a different orbit that is only transiently passing through the polar region. By restricting the sample to the re-

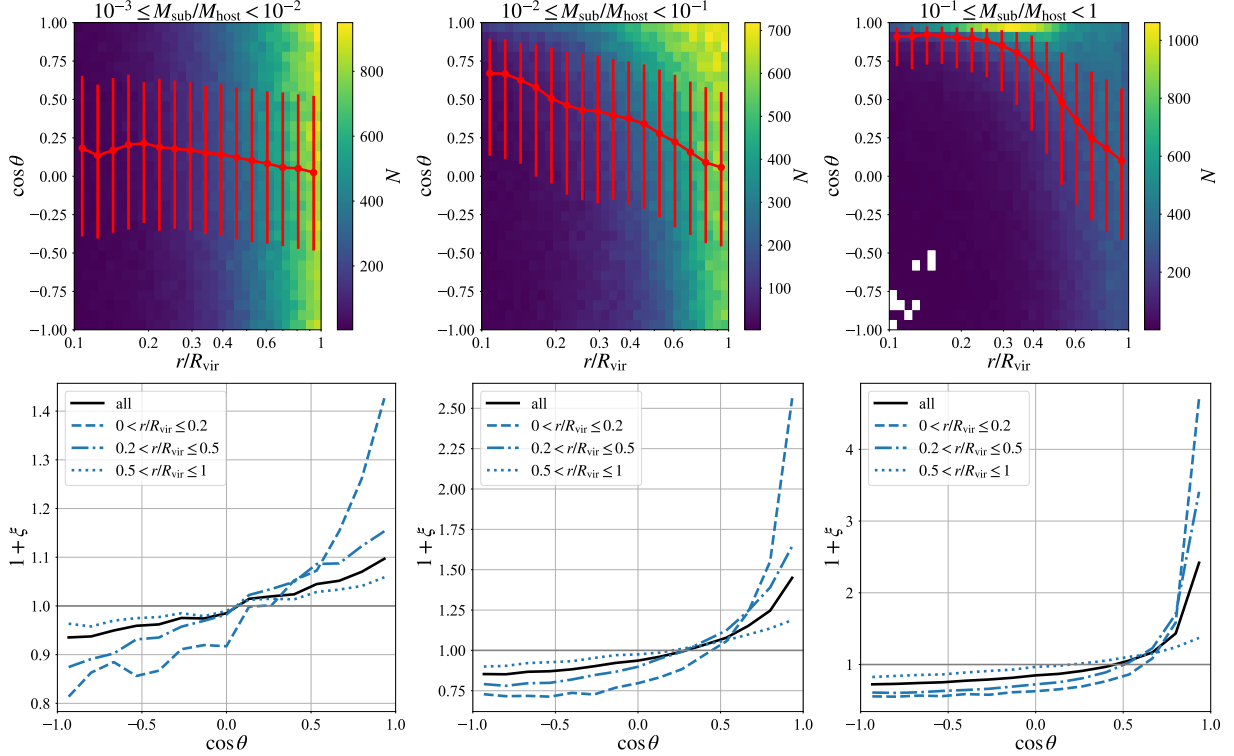


Figure 3. Upper panels: 2D histograms of $\cos \theta$ and r/R_{vir} . Lower panels: Corresponding PDFs of $\cos \theta$. Each column represents a subsample restricted by mass ratio: $10^{-3} \leq M_{\text{sub}}/M_{\text{host}} < 10^{-2}$ (left), $10^{-2} \leq M_{\text{sub}}/M_{\text{host}} < 10^{-1}$ (middle), and $10^{-1} \leq M_{\text{sub}}/M_{\text{host}} < 1$ (right).

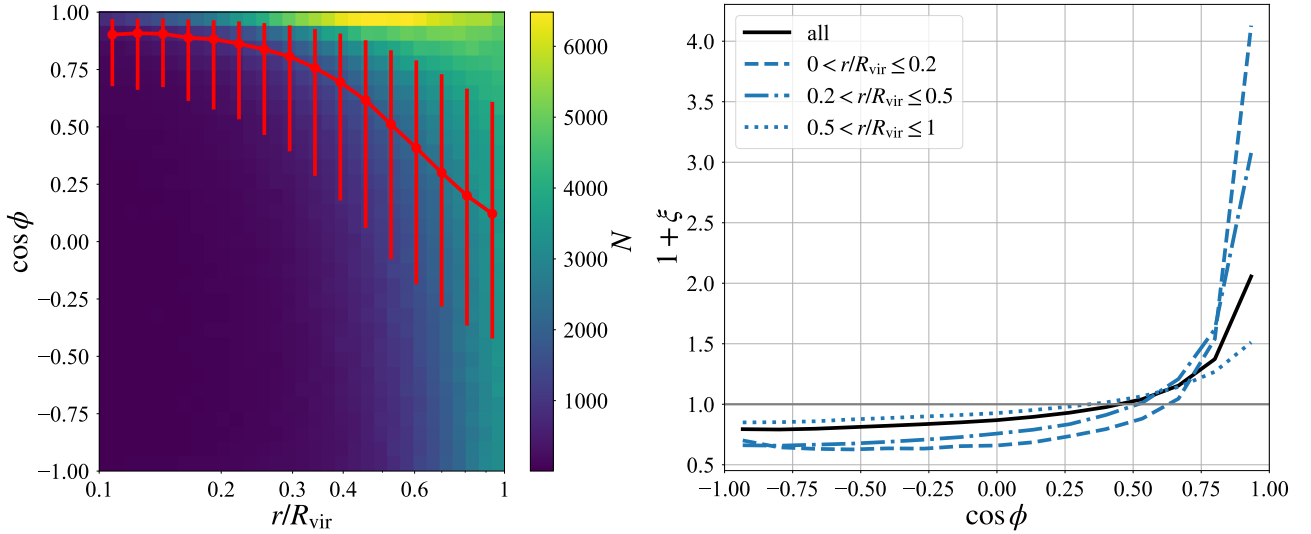


Figure 4. Same as Figure 2, but for the alignment between subhalo spin and orbital angular momentum, $\cos \phi$.

gion near the equatorial plane ($|\cos \chi| < 0.5$), we enable a robust classification of these orbits. Additionally, subhalos near the host center undergo merging processes with the host core and their position vectors \vec{X}_{sub} approach zero, making it difficult to accurately calculate

\vec{J}_{orb} . We therefore impose the constraint $r/R_{\text{vir}} > 0.1$ to ensure the reliability of our orbital calculations. Figure 5 presents 2D histograms of $\cos \theta$ and r/R_{vir} and PDFs of $\cos \theta$ for three orbital types, retrograde, polar, and prograde.

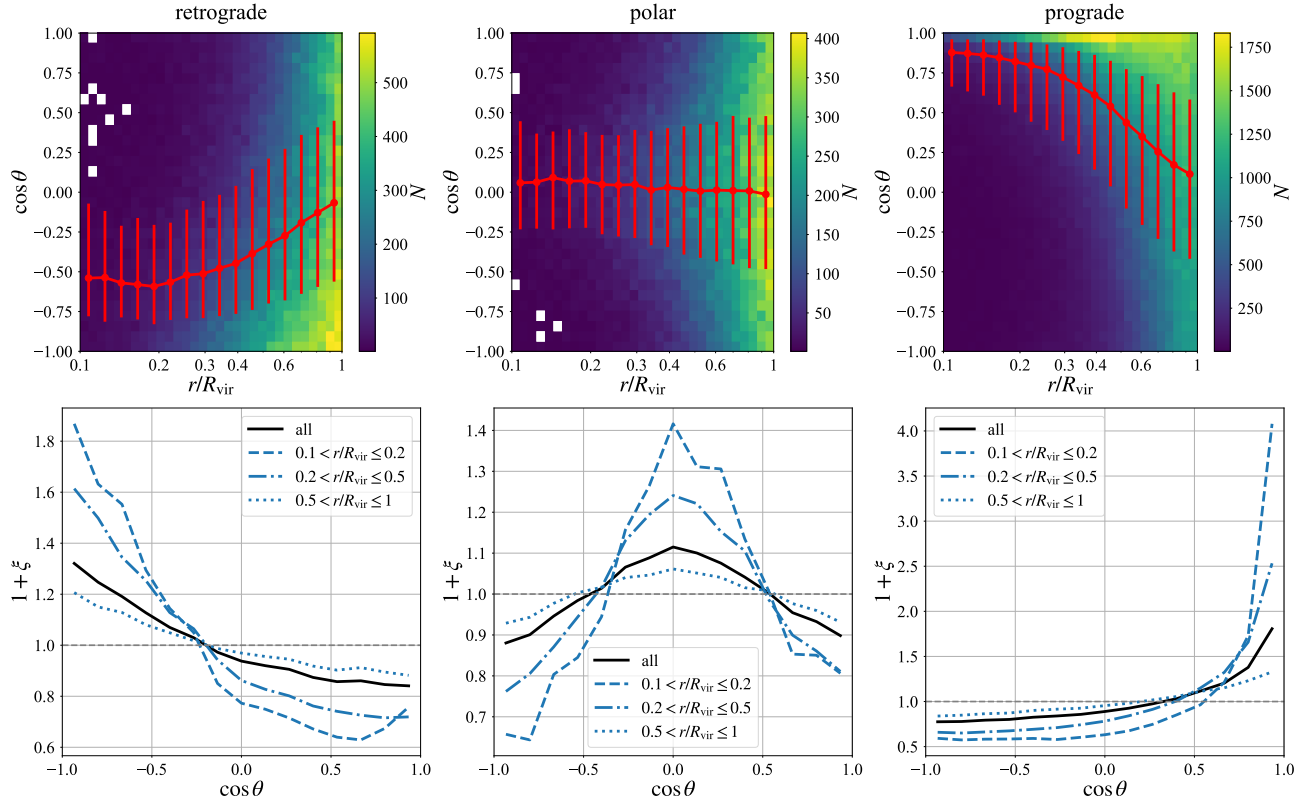


Figure 5. Upper panels: 2D histograms of $\cos\theta$ versus r/R_{vir} . Lower panels: Corresponding PDFs of $\cos\theta$. The sample is restricted to subhalos located near the equatorial plane of the host halo. The columns show results for different orbital orientation: retrograde (left, $-1 \leq \cos\eta \leq -1/3$), polar (middle, $-1/3 \leq \cos\eta < 1/3$) and prograde (right, $1/3 \leq \cos\eta < 1$). Here, $\cos\eta$ is the alignment between the subhalo orbital angular momentum \vec{J}_{orb} and the host halo spin \vec{J}_{host} .

The 2D histogram for subhalos on prograde orbits displays a clear tendency for $\cos\theta$ to increase toward the host halo center, mirroring the global trend seen in Figure 2. As shown in the PDF of prograde sample, this alignment is even more pronounced than that of the entire subhalo sample. In contrast, for polar and retrograde orbits, $\cos\theta$ values tend toward 0 and -1 , respectively, as they approach the center. This provides strong evidence for the tight alignment between spin and orbital angular momenta, as shown in Figure 4, indicating that subhalos acquire their spin through tidal torques from the host halo. Since host halos gain angular momentum through matter accretion, prograde orbits are statistically more common than retrograde ones (N. I. Libeskind et al. 2014; L. Mezini et al. 2025), leading to the emergence of the observed global spin alignment trend. In contrast, subhalos on polar and retrograde orbits acquire spins that are perpendicular and opposite to the host halo's spin direction, respectively. It is known that most subhalos with large mass ratios are prograde orbits (S.-H. An et al. 2021; L. Mezini et al. 2025), and we verified similar results. In Figure 3, the trend was more pronounced for subhalos with larger mass ratios,

suggesting that this behavior reflects the influence of their orbital angular momentum.

3.3. Dependence on accretion redshift of subhalos

Based on the tidal torquing scenario, subhalos accreted at earlier epochs are expected to exhibit more pronounced spin alignment due to prolonged tidal interactions with the host halo. We examined this by binning subhalos by their accretion redshift, z_{acc} , as shown in the $\cos\theta$ PDFs in Fig. 6. To isolate the effect of z_{acc} from mass-dependent trends, we restricted our sample to subhalos with mass ratios in the range $10^{-3} < M_{\text{sub}}/M_{\text{host}} < 10^{-2}$.

The full sample ($0 \leq r/R_{\text{vir}} < 1$) shows a weak dependence on the accretion redshift (z_{acc}). However, this dependence largely vanishes when the sample is partitioned into three radial bins. Since subhalos accreted at earlier epochs sink toward the host center via dynamical friction, the central population is inherently dominated by high- z subhalos. This suggests that the apparent z_{acc} dependence in the global sample is a manifestation of the differing radial distributions. Consequently, our results indicate that radial distance, rather than the time

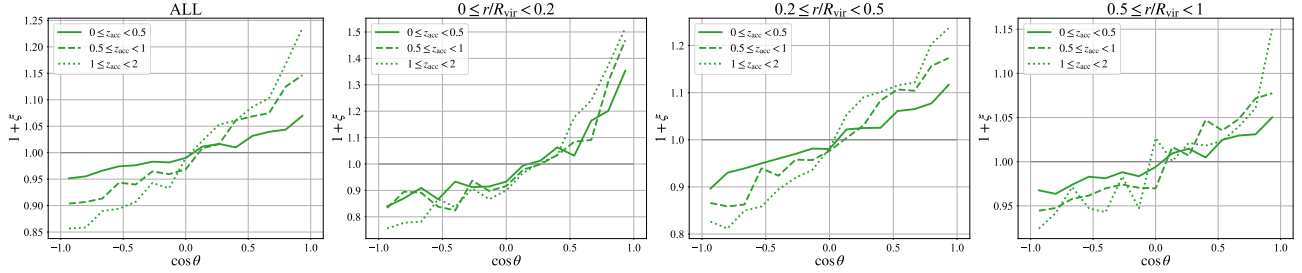


Figure 6. PDFs of $\cos \theta$ for subhalos with mass ratios $10^{-3} < M_{\text{sub}}/M_{\text{host}} < 10^{-2}$ and locations near the host equatorial plane ($|\cos \chi| < 0.5$). Each line represents a different accretion redshift (z_{acc}). From left to right, the panels correspond to the full sample ($0 \leq r/R_{\text{vir}} < 1$) and three radial subsamples: $0 \leq r/R_{\text{vir}} < 0.2$, $0.2 \leq r/R_{\text{vir}} < 0.5$, and $0.5 \leq r/R_{\text{vir}} < 1$.

elapsed since accretion, is the primary driver of subhalo spin alignment.

4. DISCUSSION AND CONCLUSION

In this study, we used the Shin-Uchuu cosmological N -body simulations to investigate the relationship between the distance from the center of the host halo and the spin direction of subhalos, focusing on subhalos surviving at $z = 0$ and tracing their accretion history back to $z = 2$. Statistically, the spin direction of subhalos exhibits an increasing tendency to align with that of their host halo as the distance to the host center decreases. This trend is driven by the observation that the orbital angular momentum of most subhalos aligns with the host halo's spin direction. As subhalos acquire spin in the same direction as their orbital angular momentum via tidal field, they consequently tend to align with the spin of the host halo. Therefore, if the orbital motion of a subhalo is misaligned with the rotation of the host halo, such as in retrograde or polar orbits, the subhalo's spin does not align with that of the host halo.

These findings provide robust evidence that subhalos acquire their spin through tidal torques from their host halos. Regarding the temporal evolution, while a weak dependence on the accretion redshift (z_{acc}) is statistically observed in the full sample, our results indicate that this is merely an apparent effect arising from differences in radial distribution. Because subhalos accreted at earlier epochs have typically sunk toward the host center due to dynamical friction, they are located in regions where alignment is naturally stronger. The fact that the z_{acc} dependence is no longer evident within individual radial bins demonstrates that the alignment strength is intrinsically linked to the distance from the host center. This confirms that radial position, rather than the time elapsed since accretion, acts as the primary driver governing subhalo spin alignment.

While subhalo major axes tend to point toward the host halo center as they approach it, a misalignment is often observed in the innermost regions ($r/R_{\text{vir}} \lesssim 0.2$) (M. J. Pereira et al. 2008; A. Knebe et al. 2008, 2020).

Our findings may help elucidate the physical mechanisms behind this central misalignment, thereby offering more profound insights into the intrinsic alignment of halos and galaxies. If the misalignment of the major axes of subhalos is indeed driven by spin, uncovering the underlying physical mechanisms will contribute to refining the probability distributions of major-axis alignments, thereby enhancing the precision of alignment models that incorporate subhalo alignment (N. Van Alfen et al. 2024).

Additionally, galaxies with low surface brightness, called ultra-diffuse galaxies (UDGs), have been observed to exhibit a tendency for high spin parameters (J. A. Benavides et al. 2023; Y. Rong et al. 2017; N. C. Amorisco & A. Loeb 2016). Investigating the influence of tidal torques on galaxy evolution may therefore help constrain the formation scenarios of UDGs.

However, since massive satellites like the LMC significantly influence subhalo orbits (E. Vasiliev 2023) and anisotropic accretion from cosmic filaments dictates the orientation of host halo spins (N. I. Libeskind et al. 2012; Y. Morinaga & T. Ishiyama 2020; P. Ganeshaiyah Veena et al. 2018, 2021), a detailed investigation of spin alignment requires a multiscale approach accounting for both cosmic filaments and individual subhalo interactions. Additionally, the spin of a galaxy does not necessarily coincide with that of its host dark matter halo (P. Bett et al. 2010). Therefore, comparing the spin acquisition of baryonic and dark matter components via hydrodynamic simulations is an essential next step.

This study has provided evidence that subhalos acquire spin through tidal torque exerted by their host halos, aligning their rotation with their orbital angular momentum. Statistically, it shows a tendency for the spin directions of subhalos and host halos to align. These findings advance our understanding of satellite galaxy formation and, by characterizing the nature of intrinsic alignment, facilitate the refinement of weak lensing analysis while mitigating associated systematic uncertainties.

ACKNOWLEDGMENTS

This work was supported by JSPS/MEXT KAKENHI Grant Numbers JP25H00671 (KW) and JP25H00662 (TI). This work was also supported by JST SPRING Grant Number JPMJSP2119, and by MEXT as a “Program for Promoting Researches on the Supercomputer Fugaku” (Toward a unified view of the Universe: from large-scale structures to planets, Grant Number JPMXP1020200109). TI has been supported by IAAR Research Support Program in Chiba University Japan, and JICFuS.

We thank Instituto de Astrofísica de Andalucía (IAA-CSIC), Centro de Supercomputación de Galicia

(CESGA) and the Spanish academic and research network (RedIRIS) in Spain for hosting Uchuu DR1 and DR2 in the Skies & Universes site for cosmological simulations. The Uchuu simulations were carried out on Aterui II supercomputer at Center for Computational Astrophysics, CfCA, of National Astronomical Observatory of Japan, and the K computer at the RIKEN Advanced Institute for Computational Science. The Uchuu DR1 and DR2 effort has made use of the skun@IAA_RedIRIS and skun6@IAA computer facilities managed by the IAA-CSIC in Spain (MICINNEU-Feder grant EQC2018-004366-P).

REFERENCES

- Amorisco, N. C., & Loeb, A. 2016, MNRAS, 459, L51, doi: [10.1093/mnrasl/slw055](https://doi.org/10.1093/mnrasl/slw055)
- An, S.-H., Kim, J., Moon, J.-S., & Yoon, S.-J. 2021, ApJ, 914, 86, doi: [10.3847/1538-4357/abfa95](https://doi.org/10.3847/1538-4357/abfa95)
- Aubert, D., Pichon, C., & Colombi, S. 2004, MNRAS, 352, 376, doi: [10.1111/j.1365-2966.2004.07883.x](https://doi.org/10.1111/j.1365-2966.2004.07883.x)
- Behroozi, P. S., Wechsler, R. H., & Wu, H.-Y. 2013a, ApJ, 762, 109, doi: [10.1088/0004-637X/762/2/109](https://doi.org/10.1088/0004-637X/762/2/109)
- Behroozi, P. S., Wechsler, R. H., Wu, H.-Y., et al. 2013b, ApJ, 763, 18, doi: [10.1088/0004-637X/763/1/18](https://doi.org/10.1088/0004-637X/763/1/18)
- Benavides, J. A., Sales, L. V., Abadi, M. G., et al. 2023, MNRAS, 522, 1033, doi: [10.1093/mnras/stad1053](https://doi.org/10.1093/mnras/stad1053)
- Bett, P., Eke, V., Frenk, C. S., Jenkins, A., & Okamoto, T. 2010, MNRAS, 404, 1137, doi: [10.1111/j.1365-2966.2010.16368.x](https://doi.org/10.1111/j.1365-2966.2010.16368.x)
- Boylan-Kolchin, M., Ma, C.-P., & Quataert, E. 2008, MNRAS, 383, 93, doi: [10.1111/j.1365-2966.2007.12530.x](https://doi.org/10.1111/j.1365-2966.2007.12530.x)
- Carlberg, R. G. 2012, ApJ, 748, 20, doi: [10.1088/0004-637X/748/1/20](https://doi.org/10.1088/0004-637X/748/1/20)
- Codis, S., Pichon, C., & Pogosyan, D. 2015, MNRAS, 452, 3369, doi: [10.1093/mnras/stv1570](https://doi.org/10.1093/mnras/stv1570)
- Fujikawa, M., & Oguri, M. 2025, arXiv e-prints, arXiv:2512.09342, doi: [10.48550/arXiv.2512.09342](https://doi.org/10.48550/arXiv.2512.09342)
- Ganeshaiah Veena, P., Cautun, M., van de Weygaert, R., Tempel, E., & Frenk, C. S. 2021, MNRAS, 503, 2280, doi: [10.1093/mnras/stab411](https://doi.org/10.1093/mnras/stab411)
- Ganeshaiah Veena, P., Cautun, M., van de Weygaert, R., et al. 2018, MNRAS, 481, 414, doi: [10.1093/mnras/sty2270](https://doi.org/10.1093/mnras/sty2270)
- Ghirardini, V., Bulbul, E., Artis, E., et al. 2024, A&A, 689, A298, doi: [10.1051/0004-6361/202348852](https://doi.org/10.1051/0004-6361/202348852)
- Hahn, O., Porciani, C., Carollo, C. M., & Dekel, A. 2007, MNRAS, 375, 489, doi: [10.1111/j.1365-2966.2006.11318.x](https://doi.org/10.1111/j.1365-2966.2006.11318.x)
- Hikage, C., Oguri, M., Hamana, T., et al. 2019, PASJ, 71, 43, doi: [10.1093/pasj/psz010](https://doi.org/10.1093/pasj/psz010)
- Hirata, C. M., & Seljak, U. 2004, PhRvD, 70, 063526, doi: [10.1103/PhysRevD.70.063526](https://doi.org/10.1103/PhysRevD.70.063526)
- Inoue, K. T., Takahashi, R., Takahashi, T., & Ishiyama, T. 2015, MNRAS, 448, 2704, doi: [10.1093/mnras/stv194](https://doi.org/10.1093/mnras/stv194)
- Ishiyama, T., Prada, F., Klypin, A. A., et al. 2021, MNRAS, 506, 4210, doi: [10.1093/mnras/stab1755](https://doi.org/10.1093/mnras/stab1755)
- Joachimi, B., Cacciato, M., Kitching, T. D., et al. 2015, SSRv, 193, 1, doi: [10.1007/s11214-015-0177-4](https://doi.org/10.1007/s11214-015-0177-4)
- Knebe, A., Yahagi, H., Kase, H., Lewis, G., & Gibson, B. K. 2008, MNRAS, 388, L34, doi: [10.1111/j.1745-3933.2008.00495.x](https://doi.org/10.1111/j.1745-3933.2008.00495.x)
- Knebe, A., Gámez-Marín, M., Pearce, F. R., et al. 2020, MNRAS, 495, 3002, doi: [10.1093/mnras/staa1407](https://doi.org/10.1093/mnras/staa1407)
- Lee, J., & Pen, U.-L. 2008, ApJ, 681, 798, doi: [10.1086/588646](https://doi.org/10.1086/588646)
- Libeskind, N. I., Hoffman, Y., Knebe, A., et al. 2012, MNRAS, 421, L137, doi: [10.1111/j.1745-3933.2012.01222.x](https://doi.org/10.1111/j.1745-3933.2012.01222.x)
- Libeskind, N. I., Knebe, A., Hoffman, Y., & Gottlöber, S. 2014, MNRAS, 443, 1274, doi: [10.1093/mnras/stu1216](https://doi.org/10.1093/mnras/stu1216)
- Lovell, M. R., Eke, V. R., Frenk, C. S., & Jenkins, A. 2011, MNRAS, 413, 3013, doi: [10.1111/j.1365-2966.2011.18377.x](https://doi.org/10.1111/j.1365-2966.2011.18377.x)
- Luo, W., Yang, X., Lu, T., et al. 2018, ApJ, 862, 4, doi: [10.3847/1538-4357/aacaf1](https://doi.org/10.3847/1538-4357/aacaf1)
- Mezini, L., Zentner, A. R., Wang, K., & Fielder, C. 2025, MNRAS, 538, 963, doi: [10.1093/mnras/staf331](https://doi.org/10.1093/mnras/staf331)
- Morinaga, Y., & Ishiyama, T. 2020, MNRAS, 495, 502, doi: [10.1093/mnras/staa1180](https://doi.org/10.1093/mnras/staa1180)
- Natarajan, P., Kneib, J.-P., Smail, I., et al. 2009, ApJ, 693, 970, doi: [10.1088/0004-637X/693/1/970](https://doi.org/10.1088/0004-637X/693/1/970)

- Okabe, N., Futamase, T., Kajisawa, M., & Kuroshima, R. 2014, ApJ, 784, 90, doi: [10.1088/0004-637X/784/2/90](https://doi.org/10.1088/0004-637X/784/2/90)
- Pereira, M. J., Bryan, G. L., & Gill, S. P. D. 2008, ApJ, 672, 825, doi: [10.1086/523830](https://doi.org/10.1086/523830)
- Planck Collaboration, Aghanim, N., Akrami, Y., et al. 2020, A&A, 641, A6, doi: [10.1051/0004-6361/201833910](https://doi.org/10.1051/0004-6361/201833910)
- Rong, Y., Guo, Q., Gao, L., et al. 2017, MNRAS, 470, 4231, doi: [10.1093/mnras/stx1440](https://doi.org/10.1093/mnras/stx1440)
- Sifón, C., Herbonnet, R., Hoekstra, H., van der Burg, R. F. J., & Viola, M. 2018, MNRAS, 478, 1244, doi: [10.1093/mnras/sty1161](https://doi.org/10.1093/mnras/sty1161)
- Van Alfen, N., Campbell, D., Blazek, J., et al. 2024, The Open Journal of Astrophysics, 7, 45, doi: [10.33232/001c.118783](https://doi.org/10.33232/001c.118783)
- van den Bosch, F. C., Tormen, G., & Giocoli, C. 2005, MNRAS, 359, 1029, doi: [10.1111/j.1365-2966.2005.08964.x](https://doi.org/10.1111/j.1365-2966.2005.08964.x)
- Vasiliev, E. 2023, Galaxies, 11, 59, doi: [10.3390/galaxies11020059](https://doi.org/10.3390/galaxies11020059)
- Wang, P. 2025, ApJL, 992, L17, doi: [10.3847/2041-8213/ae0ca5](https://doi.org/10.3847/2041-8213/ae0ca5)
- Wang, P., Guo, Q., Libeskind, N. I., et al. 2019, MNRAS, 484, 4325, doi: [10.1093/mnras/stz285](https://doi.org/10.1093/mnras/stz285)
- Welker, C., Dubois, Y., Pichon, C., Devriendt, J., & Chisari, N. E. 2018, A&A, 613, A4, doi: [10.1051/0004-6361/201629007](https://doi.org/10.1051/0004-6361/201629007)